Dalton Transactions

Influence of Nitro Substituents on the Redox, Electronic, and Proton Reduction Catalytic Behavior of Phenolate-based [N2O3]-type Cobalt(III) Complexes

Journal:	*Dalton Transactions*
Manuscript ID	DT-ART-08-2019-003158.R1
Article Type:	Paper
Date Submitted by the Author:	12-Sep-2019
Complete List of Authors:	Verani, Claudio; Wayne State University, Chemistry Basu, Debashis; Wayne State University, Chemistry Mazumder , Shivnath; Indian Institute of Technology Jammu, Department of Chemistry Kpogo, Kenneth; Wayne State Univeristy, Chemistry

Dalton Transactions

ARTICLE

Influence of Nitro Substituents on the Redox, Electronic, and Proton Reduction Catalytic Behavior of Phenolate-based $[N_2O_3]$-type Cobalt(III) Complexes

Received 00th January 20xx,
Accepted 00th January 20xx

DOI: 10.1039/x0xx00000x

www.rsc.org/

Debashis Basu,[a,b] Shivnath Mazumder,[c] Kenneth K. Kpogo,[a,d] Cláudio N. Verani*[a]

We report on the synthesis, redox, electronic, and catalytic behavior of two new cobalt(III) complexes, namely $[Co^{III}(L^1)MeOH]$ **(1)** and $[Co^{III}(L^2)MeOH]$ **(2)**. These species contain nitro-rich, phenolate-based pentadentate ligands and present dramatically distinct properties associated with the position in which the $-NO_2$ substituents are installed. Species **1** displays nitro-substituted phenolates, and exhibits irreversible redox response and negligible catalytic activity, whereas **2** has fuctionalized phenylene moieties, shows much improved redox reversibility and catalytic proton reduction activity at low overpotentials. A concerted experimental and theoretical approach sheds some light on these drastic differences.

Introduction

Interest in new 3d metal-based catalysts confirms that ligand design is essential to achieve the modulation of molecular orbital energies required for affordable redox potentials in proton and water reduction.[1-6] Similarly, the installation of substituents and their effects on the electronics of a given ligand framework enable control over the reactivity of the catalyst.[7] We have developed a phenolate-based $[N_2O_3]$ ligand originally inspired by the coordination sphere of Tyrosine Hydroxylase.[8] This ligand displays three aminophenol arms bridged by a phenylenediamine moiety, and when deprotonated it binds strongly to 3d trivalent metal ions such as $3d^3$ chromium, $3d^4$ manganese, $3d^5$ iron, $3d^6$ cobalt, and $3d^{10}$ gallium. The resulting iron(III) and gallium(III) complexes display a pentacoordinate ligand field in either trigonal bipyramidal or square pyramidal geometry and have been used in the study of molecular current rectification.[9] Cobalt(III) species have been studied for their potential as proton reduction electrocatalysts.[10,11] Indeed, these species are capable of generating dihydrogen from weak acid sources such as acetic acid, but the triply negative nature of the ligand yields fairly negative overpotentials and limits the practical use of this framework. The nature of the phenolate substituents influences

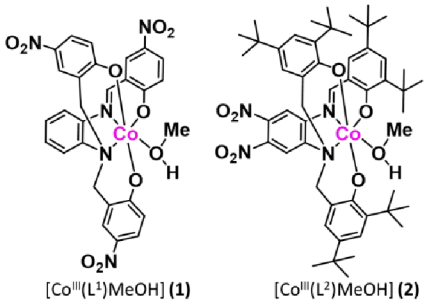

Figure 1. The mononuclear cobalt(III) complexes **1** and **2**.

[a] *Department of Chemistry, Wayne State University, Detroit, MI-48202, USA E-mail: claudio.verani@wayne.edu*
[b] *Current Address: Department of Chemistry, University of Illinois at Urbana-Champaign, Urbana, IL -61801, USA*
[c] *Department of Chemistry, Indian Institute of Technology Jammu Jammu 181221, India*
[d] *Current Address: Moses Lake Industries, Moses Lake, WA 98837*

Electronic Supplementary Information (ESI) available: Synthetic details, ^{1}H-NMR, ESI-MS spectra, crystallographic parameters, UV-visible spectra, cyclic voltammogram, redox potentials, spectroelectrochemistry, TD-DFT spectra, catalytic plots and parameters. See DOI: 10.1039/c000000x/

both redox affordability, and turnover number of the catalysts. We have learned that electron withdrawing substituents such as –Cl lead to more affordable overpotentials when compared to counterparts containing electron donating –*t*-butyl groups.[11] Based on these results we hypothesize that both the electronic nature as well as the structural position of a given substituent will have an influence on the redox, electronic, and catalytic behavior of phenolate-based [N_2O_3]-type Co(III) complexes. Thus, here we expand our work on phenolate-based cobalt(III) complexes upon the incorporation of strong electron-withdrawing nitro substituents to the ligand framework, while altering their position between the phenolate arms and the phenylene bridge. In this paper we study two new cobalt(III) complexes, namely [$Co^{III}(L^1)$MeOH] **(1)** and [$Co^{III}(L^2)$MeOH] **(2)**, shown in **Figure 1**. Species **1** displays nitro-substituted phenolates, whereas **2** has fuctionalized phenylene moieties. Results and discussion

Syntheses and characterizations. The amine proligands $H_3L^{1'}$ and $H_3L^{2'}$ were obtained by treatment of the appropriate diamine with a suitable phenolate precursor in the form of aryl chloride in presence of triethylamine (**Scheme S1**). Both species were thoroughly characterized by FTIR, ^{1}H-NMR spectroscopy, and ESI-MS spectrometry and further treated with $[Co^{II}(H_2O)_6](ClO_4)_2$ in CH_3OH and in presence of sodium methoxide as the base (**Scheme S2**). The aerobic reaction promotes metal oxidation to cobalt(III) along with conversion from amine to imine to yield [$Co^{III}(L^1)$MeOH] **(1)** and [$Co^{III}(L^2)$MeOH] **(2)**. Complexes **1** and **2** were isolated as microcrystalline samples and fully characterized by spectroscopic and spectrometric methods, as well as by elemental analyses. The FTIR spectra confirmed imine conversion with a new peak around 1600 cm^{-1}, whereas appropriate line sharpness and patterning in the ^{1}H-NMR spectra confirmed the diamagnetic nature of the 3d^6 complexes (**Figure S1**). The presence of a solvent ligand coordinated to the metal was also confirmed by ^{1}H-NMR spectroscopy. The spectrum of **2** in DMSO-d^6 is shown in **Figure 2** and exhibits appropriate line-splitting with eight aromatic protons, the azomethine proton resonance (over the aromatic region) and four methylene hydrogens between 4 and 5 ppm. Coordination of a CH_3OH molecule was confirmed by peaks at δ 3.145 ppm (-*CH*$_3$ from CH_3OH) and 4.184 (-*OH* from CH_3OH) with proton counts of three and one, respectively. Species **1** also shows CH_3OH coordination in its microcrystalline sample, but both peaks disappear upon recrystallization (**Figure S1a,b**), indicating that CH_3OH can be replaced by adventitious water. Furthermore, **2** shows intense peaks between 0 to 2 ppm due to the presence of *tert*-butyl substituents on the phenolates. ESI-MS data (**Figure S2**) showed molecular ion peaks in CH_3OH with appropriate m/z values of 638.0336 and 929.4219, respectively for $[\mathbf{1} + Na^+]^+$ and $[\mathbf{2} + Na^+]^+$, confirming once again the presence of the imine moiety. This conversion has been observed before and is well-understood.[9c]

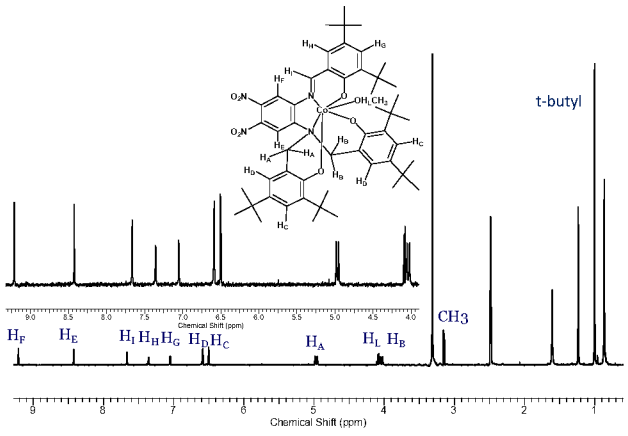

Figure 2. ^{1}H-NMR spectra for **2** in d^6-DMSO

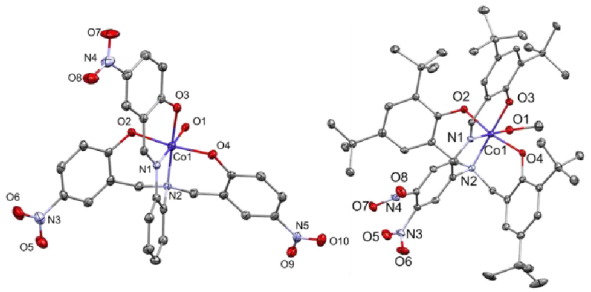

Figure 3. The ORTEP representations for **1** and **2** at 50% probability and H atoms at calculated positions. Selected bond lengths: For **1**: Co(1)-N(1): 1.874(3); Co(1)-N(2): 1.962(4); Co(1)-O(1): 1.931(3); Co(1)-O(2): 1.898 (3); Co(1)-O(3): 1.873(3); Co(1)-O(4): 1.882(3) Å; CCDC 1944910. For **2**: Co(1)-N(1): 1.875(2); Co(1)-N(2): 1.981(2); Co(1)-O(1): 1.987(2); Co(1)-O(2): 1.897(3); Co(1)-O(3): 1.875(2); Co(1)-O(4): 1.887(3) Å; CCDC 1944909.

Molecular structures. X-ray quality crystals were obtained for complexes **1** (CCDC 1944910) and **2** (CCDC 1944909), respectively from CH_2Cl_2/CH_3CN and CH_2Cl_2/CH_3OH 1:1 mixtures. Both complexes exhibited pseudo-octahedral geometry and **2** displays a CH_3OH (methanol) ligand bound to the metal at the sixth position through the protonated hydroxide (**Figure 3, S1**). The crystal structure of **1** reveals that an adventitious molecule of water replaced the original CH_3OH during recrystallization. In both complexes, the imine bond was confirmed from the presence of a shorter C-N bond (~1.3 Å), with respect to other C-N bonds (~1.5 Å). The phenylene ring, imine and one of the phenolates exhibited planarity due to extended conjugation. The two remaining phenolates are trans to each other. Hydrogen atoms were assigned to calculated positions and all the crystallographic parameters are shown in **Table T1**.

Electronic structures. UV-visible spectra were taken in CH_3CN (**Figure 4**) and CH_2Cl_2 (**Figure S3**), respectively to probe the nature of the electronic transitions in both complexes. Complex **1** is only soluble in CH_3CN, whereas complex **2** is soluble both in CH_2Cl_2 and CH_3CN. There are three major charge transfer bands in the visible region for Co^{III} complexes of similar [N_2O_3]

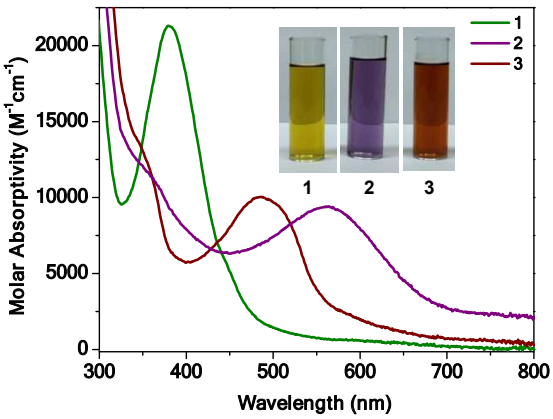

Figure 4. UV-Visible spectra for **1**-**3** in CH_3CN.

ligands;[11] Those bands are associated with phenolate to Co^{III} (LMCT) and phenolate to azomethine (LLCT) processes. The greenish-yellow $[Co^{III}(L^1)MeOH]$ **(1)** exhibited a strong band at 380 nm (ε ≈ 21,000 $M^{-1}cm^{-1}$), with a shoulder about 400 nm (ε ≈ 6,000 $M^{-1}cm^{-1}$) and a much less intense band at 607 nm (ε ≈ 1,200 $M^{-1}cm^{-1}$) in CH_3CN (**Figures 4** and **S4**). This behavior is due to a charge transfer from phenolate to cobalt and azomethine caused by the weakly donating phenolate due to the presence of strong electron-withdrawing nitro groups. TD-DFT calculations confirmed this behavior (**Figure S5**) with a calculated transition at 391 nm attributed to a phenolate-to-azomethine intraligand charge transfer (LLCT) and a calculated transition at 373 nm attributed to a ligand-to-metal charge transfer process (LMCT) involving the abovementioned $p\pi_{phenolate} \rightarrow d\sigma^*_{Co(III)}$ transition. The purple $[Co^{III}(L^2)MeOH]$ **(2)** complex shows ligand-based bands below 300 nm, along with a well-defined band at 565 nm (ε ≈ 9,400 $M^{-1}cm^{-1}$) and a smaller band at 777 nm (ε > 1,000 $M^{-1}cm^{-1}$) in CH_3CN (**Figure 4, S6**). TD-DFT calculations (**Figure S7**) associate the higher energy transition to a phenolate-to-nitro charge transfer. One new complex, $[Co^{III}(L^3)MeOH]$ (**3**) with mild electron withdrawing chloro substituents on the phenylene ring (**Figure S8-S11, Table T2,** CCDC 1944908) was synthesized to enable the comparison of electronic properties. Complex **3** displays two overlapping bands around 485 nm (ε ≈ 10,000 $M^{-1}cm^{-1}$) and 507 nm (ε ≈ 9,400 $M^{-1}cm^{-1}$), along with a weaker absorption at 762 nm (ε ≈ 650 $M^{-1}cm^{-1}$), thus showing a brown color (**Figure 4, S12**). These complexes showed similar behavior in both CH_3CN and CH_2Cl_2, as listed in **Table T3**.

Redox behavior. Cyclic voltammetry was used to gain understanding on the potentials and reversibility of metal- and ligand-centered electrochemical processes in complexes **1** and **2**. These species have shown drastically different electrochemical behaviors; Species **1** is insoluble in CH_2Cl_2 and showed mostly irreversible behavior in CH_3CN (**Figure 5, S13**), with the metal based process showing E_{pc}≈ -0.57 $V_{Fc/Fc+}$ (-0.15 $V_{Ag/AgCl}$) and E_{pa} ≈ -0.32 $V_{Fc/Fc+}$ (+0.09 $V_{Ag/AgCl}$) and a large ΔE= 0.25 $V_{Fc/Fc+}$. Other ligand-based precesses appear at less attainable potentials **(Table T4b)**. Species **2** showed rich electrochemistry with one metal-centered and four ligand-centered events in CH_3CN (**Figure 5, S14**). The Co^{III}/Co^{II} couple appeared at -0.44 $V_{Fc/Fc+}$ (-0.02 $V_{Ag/AgCl}$; ΔE: 0.17 V with E_{pc}: -0.52 and E_{pa}: -0.36; $i_{p,c}/i_{p,a}$: 0.75) as a reversible process in both solvents (**Figure S14, S15**). Two of these involve the phenolate-to-phenoxyl oxidation and two are associated with nitro-based reductions. The third phenolate/phenoxyl oxidation was observed in both CH_2Cl_2 and CH_3CN, although the equivalent reduction is sluggish, rendering the process irreversible. The imine-based process is only observed in CH_3CN (**Figure S14, S15**). The three phenolate/phenoxyl processes appeared at +0.30 $V_{Fc/Fc+}$ (0.72 $V_{Ag/AgCl}$; ΔE: 0.07 V; i_{pc}/i_{pa}: 0.91), +0.67 $V_{Fc/Fc+}$ (1.09 $V_{Ag/AgCl}$; ΔE: 0.07 V; i_{pc}/i_{pa}: 0.64), and +1.18 $V_{Fc/Fc+}$ (1.60 $V_{Ag/AgCl}$; irreversible) in CH_3CN. On the other hand, the nitro-based processes appeared at -1.24 $V_{Fc/Fc+}$ (-0.82 $V_{Ag/AgCl}$; ΔE: 0.07 V; i_{pc}/i_{pa}: 1.01) and -1.50 $V_{Fc/Fc+}$ (-1.08 $V_{Ag/AgCl}$; ΔE: 0.07 V; i_{pc}/i_{pa}: 1.38). For comparison, the chloro-containing $[Co^{III}(L^3)MeOH]$ (**3**) exhibited typical three phenolate/phenoxyl and one Co^{III}/Co^{II} redox processes both in CH_2Cl_2 and CH_3CN (**Figure S16**). Incorporation of the chloro substituents in **3** eliminated two redox processes between -1.0 and -2.0 $V_{Fc/Fc+}$, confirming the origin of those processes as nitro-based. All the CV parameters are shown in **Table T4**. DFT calculations were performed to identify origins of the redox processes for **2** in CH_3CN (**Figures 5b and 5c**). Complex **2** undergoes an $1e^-$ reduction on the $^{LS}3d^6$ cobalt(III) center (S = 0) giving rise to a $^{HS}3d^7$ Co(II) with an S = 3/2 quartet spin state. This S = 3/2 high spin state is lower in energy than the equivalent low spin S = 1/2 doublet state by 18.1 kcal/mol. In this reduction

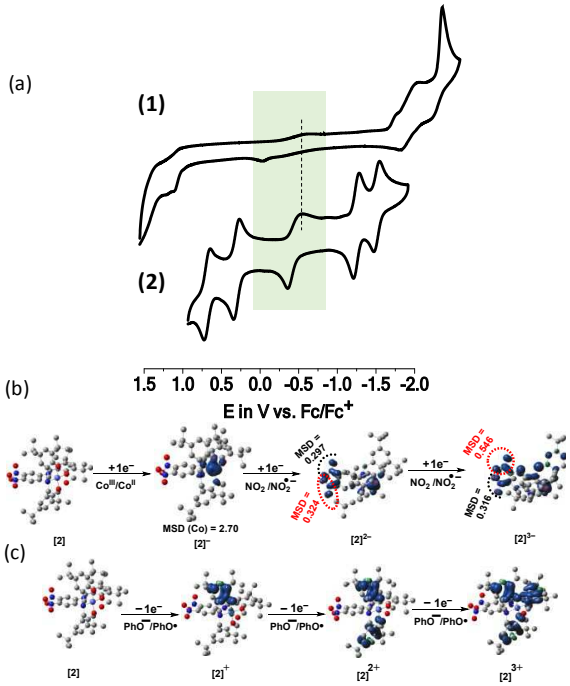

Figure 5. (a) CV for **1** and **2** in CH_3CN. The shaded area shows the metal-centered process and the dotted line coincides with the cathodic peaks for the Co^{III}/Co^{II} couples; (b) DFT-calculated spin-density plots in CH_3CN for first three reduction events; (c) first three oxidation events.

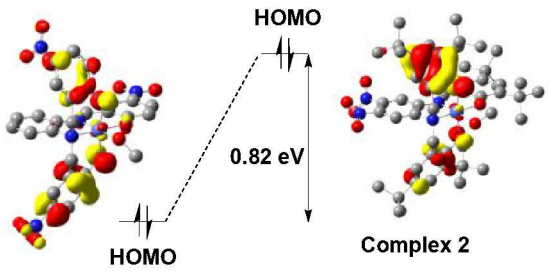

Figure 6. Comparison of DFT-calculated HOMOs for complexes **1** and **2**.

process the ^{HS}Co(II) center loses the weakly coordinating MeOH ligand and becomes five-coordinate. Contrary to the first process, the second and third reductions are based on the nitro groups of the ligand. Inspection of the Mulliken spin density (MSD) on the nitro groups in **[2]**$^{2-}$ shows that the electronic charge is delocalized over the two neighboring nitro groups. During the formation of **[2]**$^{2-}$ the —NO_2 group *para* to the imine is primarily reduced, then the *meta* —NO_2 group gets engaged in the third reduction that leads to **[2]**$^{3-}$. This *meta* group has a much larger MSD value of 0.546 compared to that in the *para* position at 0.316, and hence nearly constant to the value of 0.324 found in the previous species **[2]**$^{2-}$. However, after the third reduction **[2]**$^{3-}$ shows the electron delocalized over the imine and the phenolate ring (**Figure 5b**). While the reduction events start with a metal-based process and is followed by two ligand-based events, the oxidations involve exclusively phenolate/phenoxyl conversion (**Figure 5c**).

Spectroelectrochemical measurements were performed in order to better understand the redox processes observed for **2** (**Figure S17, S18**), in light of the DFT results.

Due to the irreversible redox profile of **1** in CH_3CN, the Co^{III}/Co^{II} cathodic peaks (E_{pc}) for **1** and **2** deliver a better basis for discussion than their $E_{1/2}$ values. These cathodic peaks appear respectively at –0.57 $V_{Fc/Fc+}$ (-0.15 $V_{Ag/AgCl}$,) and –0.52 $V_{Fc/Fc+}$ (-0.10 $V_{Ag/AgCl}$) (**Table T4)**, and therefore are quite comparable. The oxidations are reversible and allow for comparisons of $E_{1/2}$ values. In CH_3CN the potential for the first oxidation in **2** is $E_{1/2}$ = 0.30 $V_{Fc/Fc+}$ (0.72 $V_{Ag/AgCl}$), thus significantly different from the potential for the first oxidation for **1** at 1.06 $V_{Fc/Fc+}$ (1.48 $V_{Ag/AgCl}$). DFT calculations supports that the Co^{III}/Co^{II} reduction involves conversion of a low spin $3d^6$ Co^{III} into a high spin $3d^7$ Co^{II} center where both the e_g*-like MOs (d_{z2} and d_{x2-y2}) are singly occupied. Since the acceptor metal-based orbitals remain similar for both **1** and **2**, it is expected that the reduction potentials for those complexes be close to each other. However, inspection of the HOMOs which are involved in the first oxidation shows that the HOMO of **1** is delocalized over two phenolate moieties decorated with strong electron-withdrawing –NO_2 groups. In contrast, the HOMO of **2** is delocalized over two phenolate rings containing electron-donating *tert*-butyl groups (**Figure 6**). As a result, the HOMO of **2** is about 0.82 eV higher in energy than that of **1**. Consequently, **1** is more difficult to oxidize than **2**, as experimentally confirmed for the first oxidation.

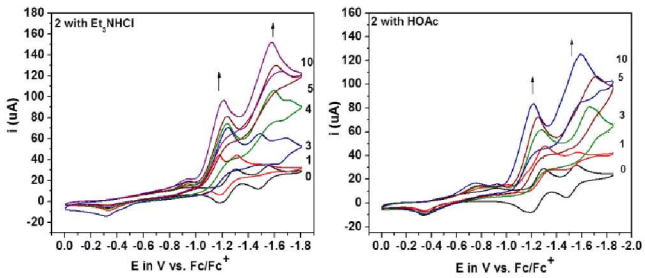

Figure 7. CV of **2** in CH_3CN in the presence of 0-10 eq. of a proton source. (a) Et_3NHCl; (b) HOAc.

Proton reduction ability. The catalytic activities of complexes **1** and **2** towards protons were investigated in presence of weak acids such as triethyl ammonium chloride (pK_a 18.7 in CH_3CN), and acetic acid (pK_a 22.3 in CH_3CN) as the proton sources. Because of the irreversible behavior for species **1** catalytic experiments were not pursued and we limit this discussion to complex **2** due to its well-behaved redox nature. Complex **2** displayed two catalytic peaks appearing around -1.21 $V_{Fc/Fc+}$ (-0.80 $V_{Ag/AgCl}$) and -1.58 $V_{Fc/Fc+}$ (-1.17 $V_{Ag/AgCl}$) in presence of Et_3NHCl (**Figure 7a**) and -1.28 $V_{Fc/Fc+}$ (-0.87 $V_{Ag/AgCl}$) and -1.64 $V_{Fc/Fc+}$ (-1.23 $V_{Ag/AgCl}$) with HOAc (**Figure 7b**). These catalytic peaks developed close to the nitro-based processes at associated overpotentials of only 0.07 V for Et_3NHCl and 0.02 V for HOAc, after considering the homoconjugation effect.[12] Thus, the electron-withdrawing and redox-active nitro group lowers the reduction potential of cobalt and imine as well as acts as an electron reservoir to reduce the catalytic overpotential. A control experiment in presence of Et_3NHCl or HOAc, but in absence of **2,** shows a catalytic peak in the blank at considerably more negative potentials of about -2.5 $V_{Fc/Fc+}$ (-2.1 $V_{Ag/AgCl}$) (**Figure S19, S20**). This result confirms the catalytic nature of **2**, and hydrogen generation was confirmed by bulk-electrolysis measurements in the presence of HOAc at an applied potential of -1.70 $V_{Ag/AgCl}$. An associated minimum TON of *ca.* 3 was determined in the presence of 100 equivalents of acid after 3 hours, with an equivalent Faradaic efficiency of 50 %. More charge was consumed during the bulk electrolysis for the complex than the blank, validating the complex as the catalyst (**Figure S21**). All catalytic parameters are listed in **Table T5**. The observation of catalysis requires some discussion. First, the TON is reported as moles of hydrogen/mole of catalyst, thus considering the full load, rather than the active amount of catalyst adsorbed onto the surface of the electrode. This leads to an underestimation of the amount of H_2 produced. Second, established mechanisms for cobalt involve variations of a sequence of events that include stepwise reduction of the $3d^6$ Co(III) precatalyst to a $3d^8$ Co(I) species that is sufficiently nucleophilic to transfer two electrons to an incoming proton, thus forming a Co(III)-H hydride. This species is usually reduced to its Co(II)-H congener, further reacting with a proton to form H_2 and regenerate the catalyst.[13,14] All reductions take place at the metal center, and the ligand has the sole function of modulating the metal reactivity. However, this landscape becomes considerably more complicated with the involvement

of the ligand in the catalytic process. From several systems investigated by our group in which ligand involvement has been confirmed,[15] a cobalt catalyst comprising of a bis-amido pyridine ligand and axial pyrrolidines[15b] may give insight. This system shows two valence tautomers at similar energies; a low-valent [Co^{I}L] and a ligand-based [Co^{II}L•] with a reduced ligand. If catalysis proceeds via [Co^{I}L], formation of a Co^{III}-H species is significantly favoured as the first step for H_2 production. On the other hand, if the [Co^{II}L•] species is involved, ligand protonation is favored leading to significant loss of planarity and pi-conjugation. Ultimately, ligand-metal bonds are broken and slow deactivation and demetallation ensues. Because we observe in **Figure 7** two catalytic waves at or below the expected potential for the Co^{II}/Co^{I} couple, ligand involvement is plausible. This might proceed in a ter Meer-like mechanism[16] in which protonation to a nitronate takes place. A dedicated effort will be necessary to outline the precise mechanism.

Conclusions

Two cobalt(III) complexes, [$Co^{III}(L^1)$MeOH] **(1)** and [$Co^{III}(L^2)$MeOH] **(2)** containing nitro-rich, phenolate-based pentadentate ligands, were synthesized and characterized by various physicochemical techniques. Remarkable differences in electronic properties were observed for **1** and **2** due to structurally distinct position of the $–NO_2$ groups in either the phenolate arms (for **1)** or the phenylene bridge (for **2**). Whereas complex **1** yielded mostly irreversible redox behavior unfit for catalysis, complex **2** displayed metal, phenolate, and nitro-based reversible processes. This complex also exhibited some proton reduction activity at the very low overpotential of 0.02 V in the presence of HOAc in CH_3CN. However, TONs are low due to ligand involvement. In fact two catalytic waves at or below the expected potential for the Co^{II}/Co^{I} couple were observed, confirming that the ligand must be reduced in order to attain catalysis. We propose that one or more $–NO_2$ groups in the reduced phenylene moiety get protonated and form nitronate groups.

In summary, we have validated our hypothesis that (i) the electronic nature and (ii) the structural position of a substituent influence the redox, electronic, and catalytic properties of phenolate-based Co(III) complexes. We have also learned that the installation of strongly electron-withdrawing groups such as $–NO_2$ lead to ligand involvement unsuitable for prolonged catalysis. New experiments will be necessary to determine the precise mechanism of deactivation, and to design catalysts with strong electron-withdrawing groups such as nitriles and carbonyls that might be less redox active.

Experimental

Materials and Methods.

General. All reagents and solvents were used as received from commercial sources. Infrared spectra were recorded from 4000 to 650 cm^{-1} as KBr pellets on a Bruker Tensor 27 FTIR spectrophotometer. ^{1}H-NMR spectroscopy was carried out with a Mercury FT-NMR 400 MHz setup using $CDCl_3$ or d^6-DMSO as solvents, at 25 °C. ESI-(+) mass spectrometry were measured in a triple quadrupole Micromass Quattro LC equipment where experimental mass patterns were fitted with theoretical isotopic distribution. Elemental analysis (C, H, and N) determinations were performed by Midwest Microlab in Indianapolis, Indiana using an Exeter analytical CHN analyzer UV–visible spectra were obtained at room temperature using a Varian Cary 50 spectrophotometer operating in the range of 200 to 1000 nm with quartz cells. Values of ε are given in M^{-1} cm^{-1}. Spectra were recorded in HPLC-grade dichloromethane (CH_2Cl_2) and acetonitrile (CH_3CN) solutions.

Electrochemistry and Spectroelectrochemistry. The electrochemical behavior of complexes **1** and **2**, as well as **3** was investigated with a BAS 50W potentiostat/galvanostat. Cyclic voltammograms were obtained at room temperature in CH_2Cl_2 and CH_3CN solutions containing 0.1 M of *n*-Bu_4NPF_6 as the supporting electrolyte under an inert argon atmosphere. The electrochemical cell was comprised of three electrodes: glassy-carbon (working), platinum wire (auxiliary) and Ag/AgCl (reference). The ferrocene/ferrocenium redox couple Fc/Fc^+ (E^o = 400 mV *vs* NHE)[17] was used as the internal standard. Peak to peak potential separations ($\Delta E_p = |E_{pc} - E_{pa}|$) and $|i_{pc} / i_{pa}|$ values were measured to evaluate the reversibility of the redox processes. Spectroelectrostatic measurements were carried out in a optically transparent thin-layer cell (*ca.* 0.1 mm) constructed according to a procedure described as follows: a flat and U-shaped platinum wire was sandwiched between two glass slides where the inner parts were coated with indium-tin oxide (ITO) (8-12 Ω/sq). The flat wire acted as the working electrode and extended outside of the slides for electrical contact. The solutions were prepared and degassed under an inert argon atmosphere and introduced into the cell through capillary action. The working electrode was located within 4-6 mm of the cell bottom to minimize ohmic potential (iR) drop. All potentials were measured *vs.* a Ag/AgCl reference electrode and a second platinum wire (counter). Potentials were applied to the cell by a BAS 50W potentiostat/ galvanostat, and the spectra were collected with a Varian Cary 50 apparatus at room temperature within a typical time interval of 30 s until the equilibrium between oxidized/reduced species was achieved.

X-ray structural determination. Diffraction data for **1** were measured on a Bruker *X8 APEX-II* kappa geometry diffractometer with Mo radiation and a graphite monochromator. Single crystals of **1** were green. A suitable crystal was selected and mounted on a Bruker APEX-II CCD diffractometer. The crystal was kept at 100.1 K during data collection. 81183 reflections were counted, which averaged to 7041 unique data (Rint = 0.1505). Using Olex2[18], the structure was solved with the olex2.solve[19] structure solution program using Charge Flipping and refined with the XL[20] refinement

package using Least Squares minimization. Hydrogen atoms were placed in calculated positions. The asymmetric unit contained one complex having a coordinated water molecule, three acetonitrile solvate at full occupancy.

Diffraction data for **2** and **3** were measured on a Bruker *X8 APEX-II* kappa geometry diffractometer with Mo radiation and a graphite monochromator. Frames were collected at 100 K with the detector at 40 mm and 0.3 degrees between each frame and were recorded for 3 s. *APEX-II*[21] and *SHELX*[20] software were used in the collection and refinement of the models.

Crystals of **2** were purple flat rods. A total of 95160 reflections was counted, which averaged to 13309 independent data (Rint = 0.14). Hydrogen atoms were placed at calculated positions. The asymmetric unit contained one complex having a coordinated methanol molecule, one methanol solvate at full occupancy, and one other solvate site described as 50/50 methanol/water. One partial occupancy carbon atom (C54) in the disordered site was held isotropic.

Crystals of the chloro-substituted **3** appeared as dark red fragments. A total of 44005 reflections was measured, yielding 11968 unique data (Rint = 0.045). Hydrogen atoms were placed in calculated positions. There was considerable disorder in the t-butyl groups. Some of these were assigned partial occupancies and held isotropic, others just retained their large thermal parameters. The complex contained one coordinated methanol, with no solvates or ions in the lattice. The highest difference peak of 1.3 e- was in the vicinity of the disordered t-butyl group.

Computational methods. Electronic structure calculations were carried out with the Gaussian 09 suite of program[22] using B3LYP functional density functional theory (DFT).[23,24] SDD basis set with an effective core potential (ECP)[25] was used for cobalt atom and 6-31G(d,p) basis set[26,27] was used for all the other atoms. All the structures were optimized in acetonitrile solvent, modeled by using SMD implicit solvation.[28] The optimized structures were confirmed to be minima on the potential energy surface by performing harmonic frequency calculations and had no imaginary normal mode frequency. Final wave functions were tested for their stability. TD-DFT calculations[29,30] in CH_3CN were performed using the same density functional and basis set. Vertical transitions with 40 excited states were calculated using ground state geometries to simulate the UV-vis spectra. The orbital transitions of the excited states were characterized using the natural transition orbital (NTO) method,[31] and the isodensity plots (isovalue = 0.04 au) of the orbitals involved in these transitions were visualized using GaussView.[32] GaussView was also used to visualize the isodensity plot of spin populations (isovalue = 0.004 au) and canonical orbitals (isovalue = 0.04 au).

Catalytic activity. Proton reduction electro-catalysis has been tested for **2** by cyclic voltammetry in presence of acetic acid (HOAc) by using glassy carbon (working), platinum wire (auxillary) and Ag/AgCl (reference) electrodes with tetra-butyl ammonium hexafluorophosphate ($TBAPF_6$) as supporting electrolyte. Overpotential (η) and i_c/i_p have been calculated from observed CV changes. Catalytic CV experiments were also performed with triethyl ammonium chloride (Et_3NHCl) for **2**.

To determine the amount of hydrogen release, bulk electrolysis was performed in a custom-made air-tight H-type cell in presence of a mercury-pool working electrode, with a Ag/AgCl reference electrode placed in the same compartment, whereas the Pt-coil auxiliary electrode was placed in the vicinal compartment separated by frit. $TBAPF_6$ was used as the supporting electrolyte. The main chamber was filled with electrolyte solution and the proton source ($TBAPF_6$: 1.560 g; HOAc: 0.024 g [0.4 mmol], 20 mL CH_3CN), and the glass-fitted chamber was filled with electrolyte solution ($TBAPF_6$: 0.390 g; 5 mL CH_3CN). In a typical test, the cell was purged with N_2 gas for 20 minutes followed by sampling head space gas (100 µL) to ensure O_2 free environment with GC. Then the solution without catalyst was electrolyzed for 3 h at -1.7 $V_{Ag/AgCl}$. The head space gas was again injected to the GC apparatus to record the amount of H_2. Then the cell was purged with N_2 gas for another 20 minutes followed by injection of the catalyst (0.004 mmol) dissolved in CH_3CN. Bulk electrolysis was conducted for another 3 h at -1.7 $V_{Ag/AgCl}$ for **2** and head space gas (100 µL) was injected to the GC to determine the amount of H_2 produced. The turnover number (TON) was calculated after background subtraction as the ratio between moles of dihydrogen produced over moles of catalyst used. Faradaic efficiency was also calculated from gas chromatography measurements. The GC is a Gow-Mac 400 with a thermal conductivity detector and 8' X 1/8" long 5Å molecular sieve column operating at 60°C was used with N_2 as the carrier gas. The calibration was carried out with H_2 gas (Hydrogen GC grade 99.99 %, Scotty analyzed gases, Sigma Aldrich).

Synthesis and Characterization.

Synthesis of the precursors.

The precursors 2-(chloromethyl)-4-nitrophenol, phenylene-diamine and 4,5-dichlorobenzene-1,2-diamine were purchased from commercial sources whereas the precursors 2,4-di-tert-butyl-6-(chloromethyl) phenol[33] and 4,5-dinitrobenzene-1,2-diamine[34] were synthesized according methods already described in the literature.

Synthesis of the amine proligands.

A general procedure is described. Phenylenediamine (2 mmol) was treated with 2-(chloromethyl)-4-nitrophenol (6.2 mmol) in presence of triethylamine (8 mmol) in 80 mL of CH_2Cl_2 for 72 h under reflux to yield a yellow colored solution. The mixture was washed three times with brine (3 × 200 mL) to remove the excess triethylamine, then dried over anhydrous sodium sulfate. The crude product was isolated by solvent rotoevaporation, and the unreacted chloride was removed by washing the solid with cold hexane to yield a yellow-colored solid. A similar procedure was followed for the reaction of 4,5-dinitrobenzene-1,2-diamine or 4,5-dichlorobenzene-1,2-diamine with 2,4-di-tert-butyl-6-(chloromethyl)phenol in presence of triethylamine in CH_2Cl_2, yielding respective red[9b] and yellow solutions.

Analyses for proligand $H_3L^{1'}$ — 2,2'-(((2-((2-hydroxy-5-nitrobenzyl)amino)phenyl)azanediyl)bis(methylene))bis(4-nitrophenol): Yield: 75%. IR (KBr, cm^{-1}) 3396(w) (OH); 3263(w) (NH); 3071(w) (Ar-CH); 2983(w), 2948(w) (alkyl-CH); 1591(m), 1490(m) (Ar-C-C); 1521(m), 1337(s), 1284(s) (-NO_2); 1162(m) (C-O). ^{1}H-NMR [400 MHz, d^6-DMSO, 300K] δ/ppm = 4.076 [s, 4H (CH_2)]; 4.372 [s, 2H (CH_2)]; 6.266 [d, 1H (aryl)]; 6.416 [t, 1H (aryl)]; 6.676 [d, 2H (aryl)]; 6.75 [t, 1H (aryl)]; 6.94 [d, 1H (aryl)]; 7.113 [d, 1H (aryl)]; 7.862 [dd, 2H (aryl)]; 7.944 [dd, 1H (aryl)]; 7.999 [d, 1H (aryl)]; 8.062 [d, 2H (aryl)]. ESI pos. in MeOH: m/z = 561.98 for $[H_3L^{1'} + H^+]^+$.

Analyses for proligand $H_3L^{2'}$ — 6,6'-(((2-((3,5-di-tert-butyl-2-hydroxybenzyl)amino)-4,5-dinitrophenyl)azanediyl) bis(methylene)) bis(2,4-di-tert-butylphenol):[9b] It was synthesized as described in reference 9b. Yield: 80%. IR (KBr, cm^{-1}) 3607(w), 3405(w) (OH); 3326(w) (NH); 3078(w) (Ar-CH); 2958(s), 2868(s) (alkyl-CH and t-bu); 1596(s), 1481(s) (Ar-C-C); 1545(s), 1364(s), 1273(s) (-NO2); 1149(m) (C-O). ^{1}H-NMR [400 MHz, $CDCl_3$, 300K] δ/ppm = 1.245 [s, 36H (t-butyl)]; 1.310 [s, 9H (t-butyl)]; 1.43 [s, 9H (t-butyl)]; 3.855 [s, 2H (CH_2)]; 4.248 [s, 2H (CH_2)]; 4.367 [s, 2H (CH_2)]; 5.691 [s, 1H (OH)]; 6.343 [s, 2H (OH)]; 6.942 [s, 1H (aryl)]; 7.031 [d, 2H (aryl)]; 7.157 [q, 3H (aryl)]; 7.329 [s, 1H (NH)]; 7.387 [d, 1H (aryl)]; 7.931 [s, 1H (aryl)]. ESI pos. in MeOH: m/z = 859.55 for $[H_3L^{2'} + Li^+]^+$.

Analyses for proligand $H_3L^{3'}$ — 6,6'-(((4,5-dichloro-2-((3,5-di-tert-butyl-2-hydroxybenzyl)amino)phenyl)azanediyl)bis (methylene))bis(2,4-di-tert-butylphenol): Yield: 85%. IR (KBr, cm^{-1}) 3612(w) (OH); 3328(w) (NH); 3070(w) (Ar-CH); 2959(s), 2906(m), 2868(m) (alkyl-CH and t-bu); 1598(w), 1482(s) (Ar-C-C); 1162(m) (C-O). ^{1}H-NMR [400 MHz, $CDCl_3$, 300K] δ/ppm = 1.244 [s, 36H (t-butyl)]; 1.323 [s, 9H (t-butyl)]; 1.426 [s, 9H (t-butyl)]; [3.803 [d, 2H (CH_2)]; 4.133 [d, 2H (CH_2)]; 4.253 [s, 2H (CH_2)]; 6.956 [s, 2H (aryl)]; 7.000 [s, 2H (aryl)]; 7.082 [s, 1H (aryl)]; 7.132 [s, 2H (aryl)]; 7.338 [s, 1H (aryl)]. ESI pos. in MeOH: m/z = 831.47 for $[H_3L^{3'} + H^+]^+$.

Synthesis of the complexes.

Complexes **1**, **2**, and **3** were synthesized under aerobic conditions using the general procedure described as follows: A 30 mL CH_2Cl_2 solution of the appropriate ligand (1 mmol) was added to a 30 mL of CH_3OH solution containing sodium methoxide (0.162 g, 3 mmol). The mixture was vigorously stirred for 10 minutes, before a 20 mL CH_3OH solution containing $[Co(H_2O)_6](ClO_4)_2$ (0.365 g, 1 mmol) was added dropwise over a period of 5 minutes. After the addition was complete, the solution was refluxed for 4 h to ensure the completion of reaction. The mixture was then concentrated to 10 mL and let to repose. Slow solvent evaporation yielded precipitates, which were collected by vacuum filtration. Further recrystallization form different solvent mixtures gave crystalline pure products.

Analyses for [Co^{III}(L^1)MeOH] **(1)•*H_2O*:** Yield. 80%. IR (KBr, cm^{-1}) 3421(w) (OH); 3063(w) (Ar-CH); 2930(w) (alkyl-CH); 1599(s), 1304(s) (NO_2); 1580(s) (C=N); 1481(s) (Ar-C-C); 1095(s) (C-O); No ClO_4^-. ^{1}H-NMR [400MHz, d^6-DMSO, 300K] δ/ppm = 3.151 [s, 3H (CH_3)]; 4.096 [s, 1H (OH)]; 4.18 [d, 2H (CH_2)]; 4.789 [d, 2H (CH_2)]; 6.398 [d, 2H (aryl)]; 7.161 [t, 1H (aryl)]; 7.375 [t, 1H (aryl)]; 7.435 [d, 1H (aryl)]; 7.554 [d, 2H (aryl)]; 7.756 [d, 1H (aryl)]; 7.801 [s, 1H (aryl)]; 8.205 [d, 1H (aryl)]; 8.260 [d, 2H (aryl)]; 8.692 [s, 1H (N=CH)];. ESI pos. in MeOH: m/z = 638.0336 for $[Co^{III}(L^1) + Na^+]^+$. Anal. Calcd for $C_{28}H_{24}CoN_5O_{11}$: C, 50.54; H, 3.64; N, 10.52. Found: C, 50.08; H, 3.87; N, 10.77. X-ray quality crystals grown from CH_2Cl_2:CH_3CN (1:1) yielded the water coordinated complex.

Analyses for [Co^{III}(L^2)MeOH] **(2)•*MeOH•½ H_2O*:** Recrystallized from CH_2Cl_2:CH_3OH (1:1). Yield. 85%. IR (KBr, cm^{-1}) 3459(w) (OH); 3060(w) (Ar-CH); 2954(s), 2868(m) (t-butyl and alkyl-CH); 1579(s) (C=N); 1541(s), 1525(s), 1360(s) (NO_2); 1473(m) (Ar-C-C); 1179(m) (C-O); No ClO_4^-. ^{1}H-NMR [400MHz, d^6-DMSO, 300K] δ/ppm = 0.849 [s, 18H (t-butyl)]; 0.987 [s, 18H (t-butyl)]; 1.218 [s, 9H (t-butyl)]; 1.590 [s, 9H (t-butyl)]; 3.145 [d, 3H (CH_3)]; 4.013 [d, 2H (CH_2)]; 4.184 [q, 1H (OH)]; 4.961 [d, 2H (CH_2)]; 6.508 [s, 2H (aryl)]; 6.579 [s, 2H (aryl)]; 7.035 [s, 1H (aryl)]; 7.345 [s, 1H (aryl)]; 7.623 [s, 1H (aryl)]; 8.380 [s, 1H (aryl)]; 9.152 [s, 1H (N=CH)]. ESI pos. in MeOH: m/z = 929.4259 for $[Co^{III}(L^2) + Na^+]^+$. Anal. Calcd for $C_{53}H_{76}CoN_4O_{9.5}$: C, 64.95; H, 7.82; N, 5.72. Found: C, 64.61; H, 7.51; N, 6.12.

Analyses for **[Co^{III}(L^3)MeOH] (3)•*1.5H_2O*.** Recrystallized from CH_2Cl_2:CH_3OH (1:1). Yield. 90%. IR (KBr, cm^{-1}) 3443(w) (OH); 3047(w) (Ar-CH); 2958(s), 2904(m), 2868(m) (t-butyl and alkyl-CH); 1605(s) (C=N); 1470(s) (Ar-C-C); 1127(m) (C-O); No ClO_4^-. ^{1}H-NMR [400MHz, d^6-DMSO, 300K] δ/ppm = 0.864 [s, 18H (t-butyl)]; 1.032 [s, 18H (t-butyl)]; 1.243 [s, 9H (t-butyl)]; 1.618 [s, 9H (t-butyl)]; 3.154 [d, 3H (CH_3)]; 3.901 [d, 2H (CH_2)]; 4.087 [q, 1H (OH)]; 4.862 [d, 2H (CH_2)]; 6.490 [s, 2H (aryl)]; 6.569 [s, 2H (aryl)]; 7.078 [s, 1H (aryl)]; 7.296 [s, 1H (aryl)]; 7.544 [s, 1H (aryl)]; 7.958 [s, 1H (aryl)]; 8.520 [s, 1H (N=CH)]. ESI pos. in MeOH: m/z = 885.3900 for $[Co^{III}(L^3) + H^+]^+$. Anal. Calcd for $C_{52}H_{74}CoN_2O_{5.5}$: C, 66.09; H, 7.89; N, 2.96 Found: C, 65.92; H, 7.52; N, 3.56

Conflicts of interest

There are no conflicts to declare.

Acknowledgements

This research was made possible by the Division of Chemical Sciences, Geosciences, and Biosciences, Office of Basic Energy Sciences of the U.S. Department of Energy (DOE-BES) through the Single-Investigator and Small-Group Research (SISGR) – Solar Energy Program Grants DE-SC0001907 and DE-FG02-09ER16120 to CNV, including financial support to DB and KK. SM acknowledges a new faculty seed grant from IIT Jammu. We thank Dr. M. J. Heeg for the collection of the raw diffractometric data sets for **2** and **3**, and the WSU-Computing Grid for high-level DFT calculations.

Notes and references

. (a) N. S. Lewis and D. G. Nocera, *Proc. Natl. Acad. Sci. U.S.A*, 2006, **103**, 15729; (b) J. A. Turner, *Science*, 2004, **305**, 972.

2. (a) L. Chen, M. Wang, F. Gloaguen, D. Zheng, P. Zhang and L. Sun, *Inorg. Chem.,* 2013, **52**, 1798; (b) M. Rose, H. B. Gray and J. R. Winkler, *J. Am. Chem. Soc.,* 2012, **134**, 8310; (c) Z. Han, W. R. McNamara, M-S Eum, P. Holland and R. Eisenberg, *Angew. Chem. Int. Ed.,* 2012, **51**, 1667; (d) M. L. Helm, M. P. Stewart, R. M. Bullock, M. R. Dubois and D. Dubois, *Science,* 2011, **333***,* 863.

3. (a) C. S. Letko, J. A. Panetiar, M. Head-Gordon and T. D. Tilley, *J. Am. Chem. Soc.*, 2014, **136**, 9364; (b) W. McNamara, Z. Han, C-J. Yin, W. W. Brennessel, P. Holland and R. Eisenberg, *Proc. Nat. Acad. Sci.,* 2012, **109**, 15594; (c) P. A. Jacques, V. Artero, J. Pecaut and M. Fontecave, *Proc. Nat. Acad. Sci.,* 2009, **106***,* 20627; (d) H. Xile, B. S. Brunschwig and J. C. Peters, *J. Am. Chem. Soc.,* 2007, **129***,* 8988; (e) C. Baffert, V. Artero and M. Fontecave, *Inorg. Chem*., 2007, **46**, 1817; (f) H. Xile, B. M. Cossairt, B. S. Brunschwig, N. S. Lewis and J. C. Peters, *Chem. Commun.,* 2005, 4723; (g) M. Razavet, V. Artero and M. Fontecave, *Inorg. Chem.,* 2005, **44,** 4786; (h) P. Connolly and J. H. Espenson, *Inorg. Chem.,* 1986, **25**, 2684.

4. (a) E. Joliat-Wick, N. Weder, D. Klose, C. Bachmann, B. Spingler, B. Probst and R. Alberto, *Inorg. Chem.*, 2018, **57**, 1651; (b) C. F. Leung, S. C. Cheng, Y. Yang, J. Xiang, S. M. Yiu, C. C. Ko and T. C. Lau, *Catal. Sci. Technol.*, 2018, **8**, 307; (c) X. Zhao, P. Wang and M. Long, *Comm. Inorg. Chem.*, 2017, **37**, 238; (d) S. Schnidrig, C. Bachmann, P. Meller, N. Weder, B. Spingler, E. Joliat-Wick, M. Mosberger, J. Windisch, R. Alberto and B. Probst, *ChemSusChem*, 2017, **10**, 4570; (e) D. Moonshiram, C. Gimbert-Suriñach, A. Guda, A. Picon, C. S. Lehmann, X. Zhang, G. Doumy, A. M. March, J. Benet-Buchholz, A. Soldatov, A. Llobet and S. H. Southworth, *J. Am. Chem. Soc.,* 2016, **138**, 10586; (f) A. Kochem, F. Thomas, O. Jarjayes, G. Gellon, C. Philouze, T. Weyhermüller, F. Neese and M. V. Gastel, *Inorg. Chem.*, 2013, **52**, 14428.

5. (a) Z. Yang, M. Pang, S-G. Xia, X-Y Gao, Q. Guo, X-B. Li, C-H Tung, L-Z Wu and W. Wang, *ChemPhotoChem*, 2019, **3**, 220; (b) J-W. Wang, K. Yamauchi, H-H. Huang, J-K. Sun, Z-M. Luo, D-C. Zhong, T-B. Lu and K. Sakai, *Angew .Chem. Int. Ed.*, 2019, **58**, 10923; (c) T. Straistari, R. Hardre, J. Fize, S. Shova, M. Giorgi, M. Reglier, V. Artero and M. Orio, *Chem. Eur. J.*, 2018, **24**, 8779; (d) M. E. Ahmed, S. Chattopadhyay, L. Wang, D. Brazzolotto, D. Pramanik, D. Aldakov, J. Fize, A. Morozan, M. Gennari, C. Duboc, A. Dey and V. Artero, *Angew .Chem. Int. Ed.*, 2018, **57**, 16001; (e) Y. Aimoto, K. Koshiba, K. Yamauchi and K. Sakai, *Chem. Commun.*, 2018, **54**, 12820; (f) L. Tong, A. Kopecky, R. Zong, K. J. Gagnon, M. S. G. Ahlquist and R. P. Thummel, *Inorg. Chem.*, 2015, **54**, 7873.

6. (a) X. Chu, J. Jin, B. Ming, M. Pang, X. Yu, C-H. Tunga and W. Wang, *Chem. Sci.*, 2019, **10**, 761; (b) R. Gueret, C. E. Castillo, M. Rebarz, F. Thomas, M. Sliwa, J. Chauvin, B. Dautreppe, J. Pécaut, J. Fortage and M-N Collomb, *Inorg. Chem.,* 2019, **58**, 9043; (c) L. Kohler, J. Niklas, R. C. Johnson, M. Zeller, O. G. Poluektov and K. L. Mulfort, *Inorg. Chem.,* 2019, **58**, 1697; (d) P. Wang, G. Liang, C. L. Boyd, C. E. Webster and X. Zhao, *Eur. J. Inorg. Chem.,* 2019, 2134; (e) P. Wang, G. Liang, M. R. Reddy, M. Long, K. Driskill, C. Lyons, B. Donnadieu, J. C. Bollinger, C. E. Webster and X. Zhao, *J. Am. Chem. Soc.,* 2018, **140**, 9219; (f) R. J. DiRisio, J. E. Armstrong, M. A. Frank, W. R. Lake and W. R. McNamara, *Dalton Trans.*, 2017, **46**, 10418; (g) D. A. Henckel, Y. F. Lin, T. M. McCormick, W. Kaminskya and B. M. Cossairt, *Dalton Trans.,* 2016, **45**, 10068; (h) W. M. Singh, T. Baine, S. Kudo, S. Tian, X. A. N. Ma, H. Zhou, N. J. DeYonker, T. C. Pham, J. C. Bollinger, D. L. Baker, B. Yan, C. E. Webster and X. Zhao, *Angew. Chem. Int. Ed.,* 2012, **51**, 5941.

7. (a) P. H. A. Kankanamalage, D. M. Ekanayake, N. Singh, A. C. P. de Morais, S. Mazumder, C. N. Verani, A. Mukherjee and M. Lanznaster, *New J. Chem.,* 2019, Accepted Manuscript DOI 10.1039/C9NJ01283D. (b) A. Call, F. Franco, N. Kandoth, S. Fernandez, M. Gonzalez-Bejar, J. Perez-Prieto, J. M. Luis and J. Lloret-Fillol, *Chem. Sci.*, 2018, **9**, 2609; (c) D. Z. Zee, T. Chantarojsiri, J. R. Long and C. J. Chang, *Acc. Chem. Res.,* 2015, **48**, 2027; (d) B. H. Solis and S. Hammes-Schiffer, *J. Am. Chem. Soc.,* 2011, **133**, 19036.

8. (a) M. Allard, J. Sonk, M. J. Heeg, B. McGarvey, H. B. Schlegel and C. N. Verani, *Angew. Chem. Int. Ed.* 2012, **51**, 3178; (b) M. Lanznaster, H. P. Hratchian, M. J. Heeg, L. Hryhorczuk, B. R. McGarvey, H. B. Schlegel and C. N. Verani, *Inorg. Chem.*, 2006, **45**, 955; (c) K. E. Goodwill, C. Sabatier and R C. Stevens, *Biochem.,* 1998, **37**, 13437.

9. (a) A. D. K. I. Weeraratne, H. Baydoun, R. Shakya, J. Niklas, L. Xie, G. Mao, S. A. Stoian, O. Poluektov and C. N. Verani, *Dalton Trans.,* 2018, **47**, 14352; (b) L. D. Wickramasinghe, S. Mazumder, K. K. Kpogo, R. J. Staples, H. B. Schlegel and C. N. Verani, *Chem. Eur. J.,* 2016*,* **22**, 10786; (c) L. D. Wickramasinghe, M. M. Perera, L. Li, G. Mao, Z. Zhou and C. N. Verani, *Angew. Chem. Int. Ed.*, 2013, **52**, 13346.

0. M. M. Allard, F. R. Xavier, M. J. Heeg, H. B. Schlegel and C. N. Verani, *Eur. J. Inorg. Chem.,* 2012, 4622.

1. D. Basu, M. M. Allard, F. R. Xavier, M. J. Heeg, R. Staples, H. B. Schlegel and C. N. Verani, *Dalton Trans.,* 2015, **44**, 3454.

2. V. Fourmond, P. A. Jacques, M. Fontecave and V. Artero, *Inorg. Chem.,* 2010, **49,** 10338.

3. D. Basu, S. Mazumder, X. Shi, H. Baydoun, J. Niklas, O. Poluektov, H. B. Schlegel and C. N. Verani, *Angew. Chem. Int. Ed.,* 2015, **54**, 2105.

14. (a) A. Bhattacharjee, E. S. Andreiadis, M. C. Kerlidou, M. Fontecave, M. J. Field and V. Artero, *Chem. Eur. J.,* 2013, **19***,* 15166; (b) J. T. Muckermann and E. Fujita, *Chem. Comm.*, 2011, **47**, 12456; (c) B. H. Solis and S. Hammes-Schiffer, *Inorg. Chem.*, 2011, **50**, 11252.

5. (a) K. K. Kpogo, S. Mazumder, D. Wang, H. B. Schlegel, A. T. Fiedler and C. N. Verani, *Chem. Eur. J.*, 2017, **23**, 9272; (b) H. Baydoun, S. Mazumder, H. B. Schlegel and C. N. Verani, *Chem. Eur. J.,* 2017, **23**, 9266; (c) D. M. Ekanayake, K. M. Kulesa, J. Singh, K. K. Kpogo, S. Mazumder, H. B. Schlegel and C. N. Verani, *Dalton Trans.*, 2017, **46**, 16812; (d) P. H. A. Kankanamalage, S. Mazumder, V. Tiwari, K. K. Kpogo, H. B. Schlegel and C. N. Verani, *Chem. Commun.*, 2016, **52**, 13357; (e) D. Basu, S. Mazumder, J. Niklas, H. Baydoun, D. Wanniarachchi, X. Shi, R. J. Staples, O. Poluektov, H. B. Schlegel and C. N. Verani, *Chem. Sci.,* 2016, **7**, 3264; (f) D. Basu, S. Mazumder, X. Shi, R. J. Staples, H. B. Schlegel and C. N. Verani, *Angew. Chem. Int. Ed.,* 2015, **54**, 7139.

6. M. F. Hawthorne, *J. Am. Chem. Soc.,* **1956**, *78,* 4980.

17. R. Gagne, C. Koval and G. Licenski, *Inorg. Chem.*, 1980, **19**, 2854.

18. O. V. Dolomanov, L. J. Bourhis, R. J. Gildea, J. A. K. Howard and H. Puschmann, *J. Appl. Cryst.*, 2009, **42**, 339.

19. L. J. Bourhis, O. V. Dolomanov, R. J. Gildea, J. A. K. Howard, and H. Puschmann, in preparation.

20. G. M. Sheldrick, *Acta Cryst*., 2008, **A64**, 112.

21. *APEX II* collection and processing programs are distributed by the manufacturer. Bruker AXS Inc., Madison WI, USA, 2009.

22. Gaussian 09, Revision D.01, M. J. Frisch, G. W. Trucks, H. B. Schlegel, G. E. Scuseria, M. A. Robb, J. R. Cheeseman, G. Scalmani, V. Barone, B. Mennucci, G. A. Petersson, H. Nakatsuji, M. Caricato, X. Li, H. P. Hratchian, A. F. Izmaylov, J. Bloino, G. Zheng, J. L. Sonnenberg, M. Hada, M. Ehara, K. Toyota, R. Fukuda, J. Hasegawa, M. Ishida, T. Nakajima, Y. Honda, O. Kitao, H. Nakai, T. Vreven, J. A. Montgomery, Jr., J. E. Peralta, F. Ogliaro, M. Bearpark, J. J. Heyd, E. Brothers, K. N. Kudin, V. N. Staroverov, T. Keith, R. Kobayashi, J. Normand, K. Raghavachari, A. Rendell, J. C. Burant, S. S. Iyengar, J. Tomasi,
M. Cossi, N. Rega, J. M. Millam, M. Klene, J. E. Knox, J. B. Cross, V. Bakken, C. Adamo, J. Jaramillo, R. Gomperts, R. E. Stratmann, O. Yazyev, A. J. Austin, R. Cammi, C. Pomelli, J. W. Ochterski, R. L. Martin, K. Morokuma, V. G. Zakrzewski, G. A. Voth, P. Salvador, J. J. Dannenberg, S. Dapprich, A. D. Daniels,

O. Farkas, J. B. Foresman, J. V. Ortiz, J. Cioslowski, and D. J. Fox, Gaussian, Inc., Wallingford CT, 2013.
23. S. H. Vosko, L. Wilk and M. Nusair *Can. J. Phys.* 1980, **58**, 1200.
24. C. Lee, W. Yang and R. G. Parr *Phys. Rev. B*. 1988, **37**, 785.
25. M. Dolg, U. Wedig, H. Stoll and H. Preuss *J. Chem. Phys.* 1987, **86**, 866.
26. P. C. Hariharan and J. A. Pople *Theor. Chim. Acta* 1973, **28**, 213.
27. M. M. Francl, W. J. Pietro, W. J. Hehre, J. S. Binkley, M. S. Gordon, D. J. DeFrees and J. A. Pople *J. Chem. Phys.* 1982, **77**, 3654.
28. A. V. Marenich, C. J. Cramer and D. G. Truhlar *J. Phys. Chem. B* 2009, **113**, 6378.
29. M. E. Casida, C. Jamorski, K. C. Casida and D. R. Salahub, *J. Chem. Phys.* 1998, **108**, 4439.
30. R. E. Stratmann, G. E. Scuseria and M. J. Frisch, *J. Chem. Phys.* 1998, **109**, 8218.
31. R. L. Martin, *J. Chem. Phys.* 2003, **118**, 4775.
32. R. Dennington, T. Keith and J. Millam, Version 5 ed.; Semichem Inc., Shawnee Mission, KS: 2009.
33. A. Sokolowski, J. Muller, T. Weyhermuller, R. Schnepf, P. Hildebrandt, K. Hildenbrand, E. Bothe and K. Wieghardt, *J. Am. Chem. Soc.*, 1997, **119**, 8889.
34. (a) A. Kleineweischede and J. Matty, *Eur. J. Org. Chem.*, 2006, 947; (b) O. Siri and P. Braunstein, *New J. Chem.*, 2005, **29**, 75.

Table of Contents

The electronic and redox properties of new two nitro-substituted cobalt species are investigated towards proton reduction.